

The clustering of the SDSS-IV extended Baryon Oscillation Spectroscopic Survey DR14 quasar sample: Anisotropic Baryon Acoustic Oscillations measurements in Fourier-space with optimal redshift weights

Dandan Wang^{1,2*}, Gong-Bo Zhao^{1,3,4†}, Yuting Wang¹, Will J. Percival⁴, Rossana Ruggeri⁴, Fangzhou Zhu⁵, Rita Tojeiro⁶, Adam D. Myers⁷, Chia-Hsun Chuang^{8,9}, Falk Baumgarten^{8,10}, Cheng Zhao¹¹, Héctor Gil-Marín^{12,13}, Ashley J. Ross^{14,4}, Etienne Burtin¹⁵, Pauline Zarrouk¹⁵, Julian Bautista⁴, Jonathan Brinkmann¹⁶, Kyle Dawson¹⁷, Joel R. Brownstein¹⁷, Axel de la Macorra¹⁸, Donald P. Schneider^{19,20}, Arman Shafieloo^{21,22}

¹ National Astronomical Observatories, Chinese Academy of Science, Beijing 100012, P.R.China

² University of Chinese Academy of Sciences, Beijing 100049, P.R.China

³ College of Astronomy and Space Sciences, University of Chinese Academy of Sciences, Beijing 100049, P.R.China

⁴ Institute of Cosmology & Gravitation, Dennis Sciama Building, University of Portsmouth, Portsmouth, PO1 3FX, UK

⁵ Department of Physics, Yale University, 260 Whitney Ave, New Haven, CT 06520, USA

⁶ School of Physics and Astronomy, University of St Andrews, North Haugh, St Andrews KY16 9SS, UK

⁷ Department of Physics and Astronomy, University of Wyoming, Laramie, WY 82071, USA

⁸ Leibniz-Institut für Astrophysik Potsdam (AIP), An der Sternwarte 16, D-14482 Potsdam, Germany

⁹ Kavli Institute for Particle Astrophysics and Cosmology & Physics Department, Stanford University, Stanford, CA 94305, USA

¹⁰ Humboldt-Universität zu Berlin, Institut für Physik, Newtonstrasse 15, D-12589 Berlin, Germany

¹¹ Tsinghua Center for Astrophysics and Department of Physics, Tsinghua University, Beijing 100084, China

¹² Sorbonne Universités, Institut Lagrange de Paris (ILP), 98 bis Boulevard Arago, 75014 Paris, France

¹³ Laboratoire de Physique Nucléaire et de Hautes Energies, Université Pierre et Marie Curie, 4 Place Jussieu, 75005 Paris, France

¹⁴ Center for Cosmology and Astro-Particle Physics, Ohio State University, Columbus, Ohio, USA

¹⁵ IRFU, CEA, Université Paris-Saclay, F-91191 Gif-sur-Yvette, France

¹⁶ Apache Point Observatory, P.O. Box 59, Sunspot, NM 88349

¹⁷ Department Physics and Astronomy, University of Utah, 115 S 1400 E, Salt Lake City, UT 84112, USA

¹⁸ Instituto de Física, Universidad Nacional Autónoma de México, Apdo.Postal 20-364, 01000, México D.F., México

¹⁹ Department of Astronomy and Astrophysics, The Pennsylvania State University, University Park, PA 16802, USA

²⁰ Institute for Gravitation and the Cosmos, The Pennsylvania State University, University Park, PA 16802, USA

²¹ Korea Astronomy and Space Science Institute, Yuseong-gu, 776 Daedeok daero, Daejeon 34055, Korea

²² University of Science and Technology, Yuseong-gu 217 Gajeong-ro, Daejeon 34113, Korea

17 January 2018

ABSTRACT

We present a measurement of the anisotropic and isotropic Baryon Acoustic Oscillations (BAO) from the extended Baryon Oscillation Spectroscopic Survey Data Release 14 quasar sample with optimal redshift weights. Applying the redshift weights improves the constraint on the BAO dilation parameter $\alpha(z_{\text{eff}})$ by 17%. We reconstruct the evolution history of the BAO distance indicators in the redshift range of $0.8 < z < 2.2$. This paper is part of a set that analyses the eBOSS DR14 quasar sample.

Key words: baryon acoustic oscillations, optimal redshift weighting, dark energy

* E-mail: ddwang@nao.cas.cn

† E-mail: gbzhao@nao.cas.cn

1 INTRODUCTION

Unveiling the underlying physics of the accelerating expansion of the universe has been one of the most challenging tasks in cosmology since its discovery from observations of supernovae (Riess et al. 1998; Perlmutter et al. 1999). Largely complementary to the supernovae, the Baryon Acoustic Oscillations (BAO), as a ‘cosmic stander ruler’, has become one of the most robust cosmological probes of the expansion history of the Universe since it was first detected (Cole et al. 2005; Eisenstein et al. 2005) from large scale galaxy surveys.

To map the evolution of the cosmic expansion, which is crucial to study the nature of dark energy, BAO measurements at various cosmic epochs are required (Zhao et al. 2012, 2017a). However, it is challenging to extract the tomographic BAO information from a galaxy survey, as usually one has to combine galaxies from a range of redshifts to obtain a robust BAO measurement at one, or a small number of *effective* redshifts. For example, the SDSS-III BOSS (Eisenstein et al. 2011; Dawson et al. 2012) survey has successfully obtained a per cent level accuracy BAO measurement, but only at three effective redshifts in the range of $0.2 < z < 0.75$ (Alam et al. 2017).

To extract the lightcone information, one can decompose the survey into a large number of overlapping redshift slices, and perform the BAO analysis in each redshift bin, and every pair of redshift bins to quantify the covariance (Zhao et al. 2017b; Wang et al. 2017). However, this approach is computationally expensive, and is likely to be impractical for future deep surveys such as DESI or Euclid.

A more efficient approach is to assign each galaxy an additional weight, according to its redshift, and optimise the weight so that a high level of tomographic information can be extracted at a low computational cost. Early applications of the optimal redshift weight for a BAO measurement were made by Zhu et al. (2015); Zhu et al. (2016) in configuration space using two-point correlation functions. In this work, we adopt a complementary approach to perform a new BAO analysis with optimal redshift weights in Fourier space, and apply our technique to the extended Baryon Oscillation Spectroscopic Survey (eBOSS) (Dawson et al. 2016) Data Release 14 (DR14) quasar (QSO) sample.

The structure of this paper is as follows. We introduce the DR14 quasar catalogue and mocks used in this work in Section 2; then in Section 3, we describe details of the methodology, including the derivation of the redshift weights for power spectrum multipoles, the measurement of the weighted sample, the template, and fitting procedure used for this analysis. We present our main results in Section 4, followed by a conclusion and discussion in Section 5.

2 THE DR14 QSO AND MOCK SAMPLES

eBOSS (Dawson et al. 2016) is a cosmological survey of the SDSS-IV project (Blanton et al. 2017), which uses the 2.5-meter Sloan Telescope (Gunn et al. 2006) with the BOSS double-armed spectrographs (Smee et al. 2013). The eBOSS DR14 quasar catalogue (Pâris et al. 2017; Abolfathi et al. 2017) that we use contains quasars from the first two years of eBOSS observations, which are limited to a redshift range of $0.8 < z < 2.2$. The catalogue covers 1214.64 deg^2 in the North Galactic Cap (NGC), and 898.27 deg^2 in the South Galactic Cap (SGC). There are 95161 and 63596 effective quasars in the NGC and SGC, respectively. The effective volume is $5.44 \times 10^7 (h^{-1} \text{ Mpc})^3$ and $3.34 \times 10^7 (h^{-1} \text{ Mpc})^3$ for the NGC and SGC, respectively. The redshifts are adopted from the SDSS quasar pipeline (Z_{PL}) with visual inspections.

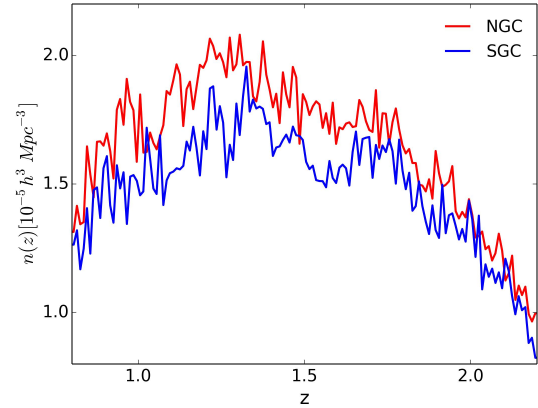


Figure 1. The redshift distribution for the DR14 QSO sample in the NGC (red) and SGC (blue).

	Ω_m	Ω_Λ	$\Omega_b h^2$	h
Fiducial	0.31	0.69	0.022	0.676
EZmock	0.307	0.693	0.02214	0.676

Table 1. The fiducial cosmological model of this paper, the cosmology used in creating the EZ mocks.

Fig 1 shows the redshift distribution of the quasar sample. There is a slight difference in the NGC and the SGC, because the targeting efficiency in these two regions is slightly different. More details of the target selection can be found in Myers et al. (2015).

Each quasar in the DR14 quasar catalogue is assigned a product of a few different weights, namely, w_{sys} , w_{cp} , w_{focal} and w_{FKP} , where w_{sys} is the systematic weight correcting for effects such as Galactic extinction and the limiting magnitude; the close pair weight w_{cp} and the focal plane weight w_{focal} correct for redshift failures and fibre collisions, and the FKP weight w_{FKP} minimises the uncertainty of power spectrum measurement as introduced by Feldman et al. (1994),

$$w_{\text{FKP}} = \frac{1}{1 + \bar{n}(z)P_0} \quad (1)$$

where P_0 is the amplitude of power spectrum in k space, which is fixed to $6000 h^{-3} \text{ Mpc}^3$ in this paper. In addition, we assign each quasar a redshift weight w_z , which is detailed in Section 3.1. Thus the total weight for each quasar is

$$w_{\text{tot}} = w_{\text{sys}} w_{\text{cp}} w_{\text{focal}} w_{\text{FKP}} \sqrt{w_z}. \quad (2)$$

We use 1000 EZmocks (Chuang et al. 2015) to compute the data covariance matrix and for mock tests. EZmocks has the lightcone information, which allows one to investigate the redshift evolution of the clustering of quasars. The fiducial cosmology used for EZmocks is given in Table 1.

3 METHODOLOGY

3.1 The optimal redshift weights

In this section, we present details of the algorithm of optimal redshift weighting for BAO analysis in Fourier space.

We use the parametrisation of the distance-redshift relation described in [Zhu et al. \(2015\)](#),

$$\frac{\chi(z)}{\chi_{\text{fid}}(z)} = \alpha_0 \left(1 + \alpha_1 x + \frac{1}{2} \alpha_2 x^2 + \dots \right) \quad (3)$$

where $x = \chi_{\text{fid}}(z)/\chi_{\text{fid}}(z_0) - 1$, the subscript ‘fid’ denotes the fiducial cosmology (Table 1). As demonstrated in [Zhu et al. \(2016\)](#), Eq (3) can accurately parametrise $\chi(z)$ for a wide range of cosmologies. In this work, we set the pivot redshift z_0 to be the effective redshift of the quasar sample, *i.e.*, $z_0 = 1.52$.

The transverse and the radial BAO dilation parameters α_{\perp} and α_{\parallel} are,

$$\begin{aligned} \alpha_{\perp} &= \alpha_0 \left(1 + \alpha_1 x + \frac{1}{2} \alpha_2 x^2 \right) \\ \alpha_{\parallel} &= \alpha_0 \left(1 + \alpha_1 + (2\alpha_1 + \alpha_2) x + \frac{3}{2} \alpha_2 x^2 \right) \end{aligned} \quad (4)$$

The optimal redshift weight of α_i can be evaluated as follows ([Zhu et al. 2015](#)),

$$w_{\ell,i} = C^{-1} P_{\ell,i}$$

where ℓ refers to the power spectrum multipole, and C is the data covariance matrix,

$$C = \left(P + \frac{1}{\bar{n}} \right)^2 dV$$

The diagonal elements of C^{-1} essentially represent the effective volume of the survey at various redshifts. As the light-cone of EZmocks is assembled by snapshots at seven redshifts, we split the entire redshift range into seven slices, and compute $\bar{n}(z)$ in each redshift slice.

The quantity $P_{\ell,i}$ is the derivative of the power spectrum multipole with respect to α_i , which can be evaluated analytically,

$$\frac{\partial P_{\ell}(k, z)}{\partial \alpha_i} = \frac{\partial P_{\ell}(k, z)}{\partial \alpha_{\parallel}} \frac{\partial \alpha_{\parallel}}{\partial \alpha_i} + \frac{\partial P_{\ell}(k, z)}{\partial \alpha_{\perp}} \frac{\partial \alpha_{\perp}}{\partial \alpha_i}$$

where $P_{\ell}(k, z)$ is the ℓ^{th} power spectrum multipole at wavenumber k and redshift z , as detailed in Section 3.3.1.

Given Eq (4), it is straightforward to obtain several of the derivative terms analytically,

$$\frac{\partial \alpha_{\perp}}{\partial \alpha_0} = 1; \quad \frac{\partial \alpha_{\parallel}}{\partial \alpha_0} = 1$$

$$\frac{\partial \alpha_{\perp}}{\partial \alpha_1} = x; \quad \frac{\partial \alpha_{\parallel}}{\partial \alpha_1} = 1 + 2x$$

$$\frac{\partial \alpha_{\perp}}{\partial \alpha_2} = \frac{1}{2} x^2; \quad \frac{\partial \alpha_{\parallel}}{\partial \alpha_2} = x + \frac{3}{2} x^2 \quad (5)$$

and the terms $\frac{\partial P_{\ell}(k, z)}{\partial \alpha_{\perp}}$ and $\frac{\partial P_{\ell}(k, z)}{\partial \alpha_{\parallel}}$ can be evaluated numerically¹.

These weights are generally functions of z and k , we have

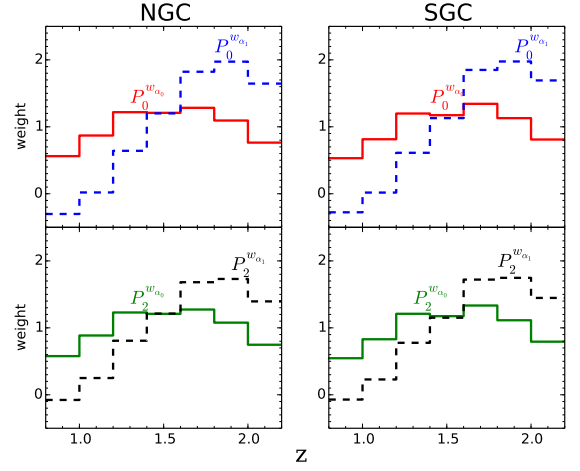


Figure 2. The optimal redshift weights derived from power spectra multipoles measured in NGC (left) and SGC (right), respectively. In all panels, weights for α_0 and α_1 are shown in solid and dashed lines respectively.

numerically checked that the k -dependence of the weights and the dependence is so weak in the k range of interest that we drop the k -dependence for simplicity, and evaluate the weights at $k = 0.1 \text{ h Mpc}^{-1}$.

The resultant redshift weights are shown in Fig 2². The weights for the monopole and quadrupole are similar, and they all peak at the effective redshift. This behavior is expected as P_0 and P_2 evolve with redshift in similar ways³, and the monopole is most sensitive to an isotropic BAO shift parametrised by α_0 at the effective redshift, where the monopole has the largest signal to noise ratio. On the other hand, power spectra at high redshifts are more useful to measure α_1 , as it is apparent from Eq (4) that the effect of α_1 on the BAO measurement is maximised at high z . This is the reason why the weights for α_0 peak at high redshifts.

3.2 Measurements of the power spectra multipoles

To apply the redshift weights to the quasar and random catalogues, we first perform a linear transformation of the weights to get a set of positive-definite new weights, which is required as the weight assigned to each quasar is the square root of the z -weights derived previously. As this is a linear operation, this transformation preserves the information content.

To measure the power spectrum multipoles from the z -weighted DR14 quasar catalogue and each of the EZ mock catalogues, we adopt the method detailed in [Zhao et al. \(2017b\)](#), which is based on a Fast Fourier Transform (FFT) method ([Bianchi et al. 2015](#)). We embed the entire survey volume into a cubic box with size of $8000 \text{ h}^{-1} \text{ Mpc}$ a side, and subdivide it into $N_g = 1024^3$ grids. We use the Piecewise Cubic Spline (PCS) interpolation to smooth the overdensity field to reduce the aliasing effect when assigning the quasar samples and randoms to the grids, [Sefusatti et al. \(2016\)](#).

We measure the multipoles up to $k = 0.3 \text{ h Mpc}^{-1}$ with $\Delta k = 0.01 \text{ h Mpc}^{-1}$. Fig. 3 displays the power spectrum monopole and

² We derive the weights at the resolution of $\Delta z = 0.2$ as this bin size is the redshift resolution used to generate the lightcone for the EZ mocks.

³ P_0 and P_2 evolve in exactly the same way in linear perturbation theory.

¹ These terms can also be evaluated analytically with approximations ([Ruggeri et al. 2017](#)).

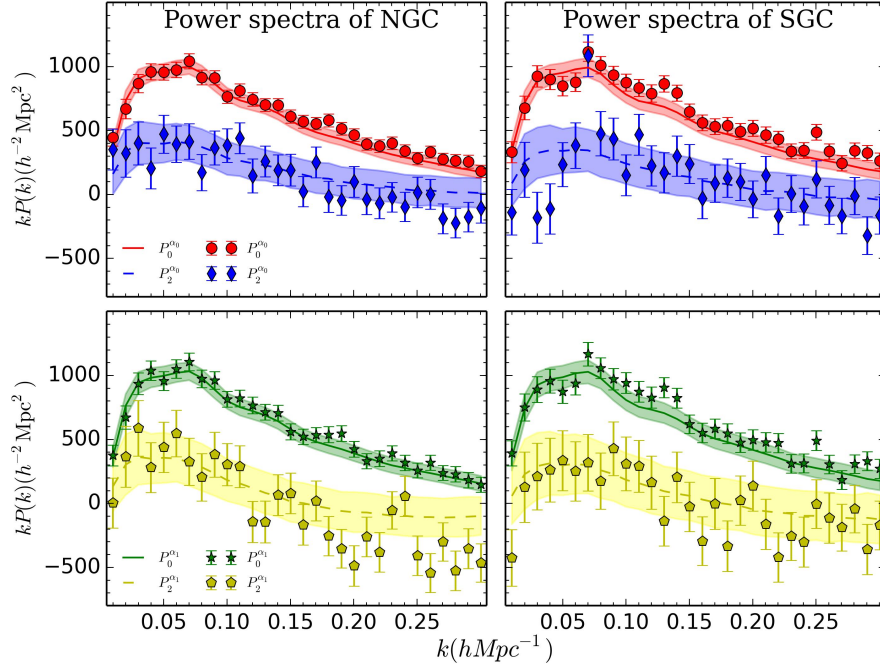


Figure 3. The power spectrum monopole and quadrupole measured from the DR14 quasar catalogue (data points with error bars) and from 1000 EZmocks (shaded bands) weighted by the optimal redshift weights for α_0 (upper panels) and α_1 (lower) in the NGC (left panels) and SGC (right) respectively.

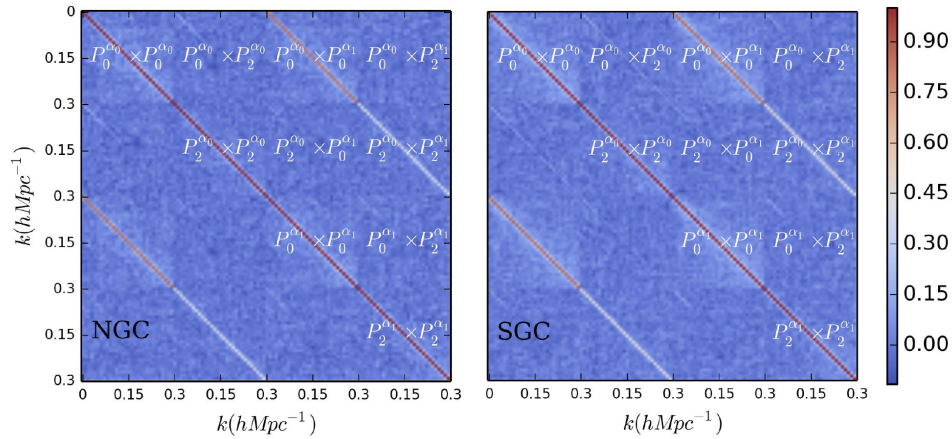


Figure 4. The correlation matrix among power spectra monopole and quadrupole weighted by α_0 and α_1 in the NGC (left) and SGC (right), respectively.

quadrupole weighted for α_0 and α_1 in both NGC and SGC. The observables in the NGC and SGC are consistent within the error bars derived from the EZ mocks.

The data covariance matrix is computed as,

$$C_{ij, \alpha_m \alpha_n}^{\ell \ell'} = \frac{1}{N_{\text{mock}} - 1} \sum_{q=1}^{N_{\text{mock}}} \left[P_{\ell, \alpha_m}^q(k_i) - \bar{P}_{\ell, \alpha_m}(k_i) \right] \times \left[P_{\ell', \alpha_n}^q(k_j) - \bar{P}_{\ell', \alpha_n}(k_j) \right] \quad (6)$$

$$\bar{P}_{\ell, \alpha_m}(k_i) = \frac{1}{N_{\text{mock}}} \sum_{q=1}^{N_{\text{mock}}} P_{\ell, \alpha_m}^q(k_i) \quad (7)$$

where $N_{\text{mock}} = 1000$, i denotes the i^{th} k -bin, ℓ denotes order of the power spectrum multipole, and m runs over 0, 1.

We use the Hartlap factor f_{H} to correct for the bias of the inverse of the maximum-likelihood estimator of the covariance matrix (Hartlap et al. 2006). The factor f_{H} is defined as,

$$f_{\text{H}} = \frac{N_{\text{mock}} - N_{\text{b}} - 2}{N_{\text{mock}} - 1}$$

where N_{b} is the number of k -bins used for analysis. The corrected inverse matrix of the covariance matrix is,

$$\tilde{C}_{ij}^{-1} = f_{\text{H}} C_{ij}^{-1}$$

The corresponding data correlation matrices for these observables, which are the normalised data covariance matrices with all the diagonal elements being unity, for these observation, are presented in Fig 4. The α_0 and α_1 weighted monopoles correlate with each other (at the same k mode) to a large extent, thus it is difficult to constrain α_0 and α_1 simultaneously using the monopole alone. However, the correlation for the quadrupole is much less; adding quadrupole to the analysis can assist in breaking the degeneracy between α_0 and α_1 .

3.3 The BAO analysis

3.3.1 The template

The template we chose to model the z -dependent two-dimensional quasar power spectrum is,

$$P_g(k, \mu, z) = P_{\text{nw, lin}}(k, \mu, z) \left[b(z) + f(z) \mu^2 \right]^2 \left[1 + O_{\text{lin}}(k) e^{-k^2(\mu^2 \Sigma_{\parallel}^2 + (1-\mu^2) \Sigma_{\perp}^2)/2} \right] \quad (8)$$

$$P_{\text{nw, lin}}(k, z) = \left[\frac{D(z)}{D(z=z_0)} \right]^2 P_{\text{nw, lin}}(k, z_0) \quad (9)$$

where $D(z)$ is the growth function. We follow Ata et al. (2018) and fix Σ_{\perp} to $7.8 h^{-1}$ Mpc and Σ_{\parallel} to $5.2 h^{-1}$ Mpc at the effective redshift.

We model the time evolution of the linear bias using the quadratic function of $b(z) = 0.53 + 0.29(1+z)^2$ (Croom et al. 2005), which has been confirmed to be a reasonable model for the eBOSS DR14 sample (Laurent et al. 2017). The linear growth rate $f(z)$ is modelled follows Linder (2005),

$$f(z) = \left[\frac{\Omega_m(1+z)^3}{\Omega_m(1+z)^3 + 1 - \Omega_m} \right]^{\gamma}$$

where the gravitational growth index γ is fixed to 0.545.

The multipole can be calculated from,

$$P_{\ell}(k, z) = \frac{2\ell + 1}{2\alpha_{\perp}^2 \alpha_{\parallel}} \int P_g(k', \mu', z) \mathcal{L}(\mu) d\mu \quad (10)$$

$$+ \frac{a_{\ell 1}}{k^3} + \frac{a_{\ell 2}}{k^2} + \frac{a_{\ell 3}}{k} + a_{\ell 4} + a_{\ell 5} k \quad (11)$$

with

$$k' = \frac{k}{\alpha_{\perp} \sqrt{1 + \left[\left(\frac{\alpha_{\perp}}{\alpha_{\parallel}} \right)^2 - 1 \right] \mu^2}}$$

$$\mu' = \frac{\mu}{\frac{\alpha_{\parallel}}{\alpha_{\perp}} \sqrt{1 + \left[\left(\frac{\alpha_{\perp}}{\alpha_{\parallel}} \right)^2 - 1 \right] \mu^2}} \quad (12)$$

to encode the Alcock-Paczynski effect (Alcock & Paczynski 1979), where

$$\alpha_{\perp} = \frac{D_A(z) r_{\text{d}}^{\text{fid}}}{D_A^{\text{fid}}(z) r_{\text{d}}}; \quad \alpha_{\parallel} = \frac{H^{\text{fid}}(z) r_{\text{d}}^{\text{fid}}}{H(z) r_{\text{d}}}$$

and the polynomial is to marginalised over the broad band shape.

The z -weighted template is,

$$P_{\ell}^{\text{W}i}(k) = \int w_{\ell, \alpha_i}(z) P_{\ell}(k, z) dz \quad (13)$$

3.3.2 Parameter estimation

We perform the parameter estimation using a modified version of CosmoMC, which is a Markov Chain Monte Carlo (MCMC) (Lewis & Bridle 2002) engine for cosmological parameter constraints. We minimise the following χ^2 in the global fitting,

$$\chi^2 = (D + X)^T C^{-1} (D + X)$$

where D is the difference vector defined as $D(k) \equiv P^{\text{data}}(k) - P^{\text{theo}}(k)$, and C is the covariance matrix for the weighted power spectra multipoles. We follow the method presented in Zhao et al. (2017) to analytically marginalise over the nuisance parameters $a_{\ell i}$. We correct for the bias due to our finite number of mocks by rescaling the inverse data covariance matrix by the M factor (Percival et al. 2014),

$$M = \sqrt{\frac{1 + B(N_{\text{b}} - N_{\text{p}})}{1 + A + B(N_{\text{p}} + 1)}}$$

with

$$A = \frac{2}{(N_{\text{mock}} - N_{\text{b}} - 1)(N - N_{\text{b}} - 4)}$$

$$B = \frac{N_{\text{mock}} - N_{\text{b}} - 2}{(N_{\text{mock}} - N_{\text{b}} - 1)(N_{\text{mock}} - N_{\text{b}} - 4)}$$

where N_{p} is the number of parameters and N_{b} is the number of k -bins used in the analysis.

4 RESULTS

We fit α_0 and α_1 to the observables derived from both the EZ mocks and from the DR14 quasar sample using our template with redshift weights discussed in Sec. 3.3.1, setting k_{max} to $0.23 h \text{Mpc}^{-1}$ as the fiducial case. For comparison, we perform separate analyses in

Model	α_1	α_0 ($\alpha_\perp(z_{\text{eff}})$)	$\alpha_{\parallel}(z_{\text{eff}})$	$\alpha(z_{\text{eff}})$	$\text{corr}(\alpha_0, \alpha_1)$	$\text{corr}(\alpha_\perp(z_{\text{eff}}), \alpha_{\parallel}(z_{\text{eff}}))$	χ^2/DoF
Averaged mocks							
Fiducial	-0.001 ± 0.252	1.000 ± 0.086	0.999 ± 0.213	1.000 ± 0.063	-0.585	-0.299	–
DR14 QSO sample							
Fiducial	-0.038 ± 0.125	1.037 ± 0.059	0.998 ± 0.097	1.024 ± 0.040	-0.723	-0.376	122/138
w/o z-weights	-0.016 ± 0.130	1.027 ± 0.069	1.011 ± 0.090	1.022 ± 0.048	-0.793	-0.419	56/66
$k_{\text{max}} = 0.30 h \text{ Mpc}^{-1}$	-0.026 ± 0.118	1.030 ± 0.055	1.003 ± 0.095	1.021 ± 0.038	-0.667	-0.284	164/194

Table 2. Constraints on BAO parameters derived from the average of the EZ mocks (upper part of the table) and the DR14 quasar catalogue (lower). The analysis is performed with redshift weights using the k modes in the range of $0.01 < k < 0.23 h \text{ Mpc}^{-1}$. To be imaginable, we also show α_\perp , α_{\parallel} and their correlation at the effective redshift, where α_\perp is the same as α_0 .

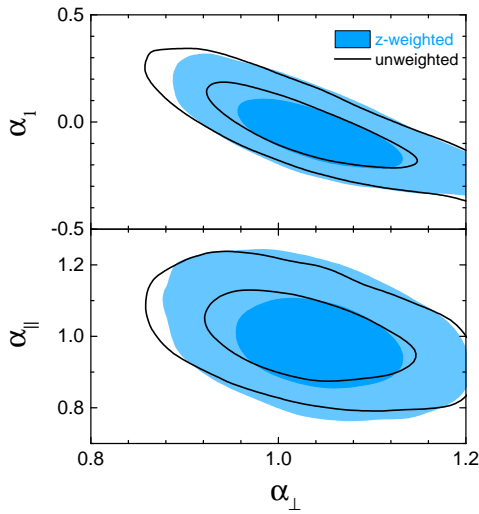


Figure 5. The 68 and 95% CL contour plots for $\alpha_0(\alpha_\perp(z_{\text{eff}}))$, α_1 and $\alpha_{\parallel}(z_{\text{eff}})$ with (blue filled) and without (black unfilled) the redshift weights.

another two cases in which the redshift weights are not applied, or k_{max} is set to $0.3 h \text{ Mpc}^{-1}$.

The result of the mock test is listed in the upper section of Table 2. The recovered values of the parameters from the mocks are in excellent agreement with the expected values of $\alpha_0 = 1$, $\alpha_1 = 0$ in the fiducial case. We derive the constraints on α_\perp , α_{\parallel} and the isotropic BAO dilation parameter $\alpha \equiv \alpha_\perp^{2/3} \alpha_{\parallel}^{1/3}$ from α_0 and α_1 , and quantify the correlation among these parameters.

We then apply our pipeline to the DR14 quasar sample, and present the results in the lower part of Table 2 in cases of fiducial, no redshift weights, and with k_{max} extended to $0.3 h \text{ Mpc}^{-1}$. The results are illustrated in Figs 5 and 6. Our investigation reveals that,

- The redshift weights generally improve the constraints, with the uncertainty of α_0 (α_\perp) and α_1 improved by 4% and 14%, respectively. The uncertainty of the derived isotropic α are tightened by 17%. The improvement is also visible from Fig 5, in which the 68 and 95% confidence interval (CL) contours between α_\perp , α_{\parallel} and α_1 are shown;
- The constraint on the derived α_{\parallel} is not improved by the redshift weights. That is probably because the redshift weights reduce the correlation between α_0 and α_1 . This result explains why the

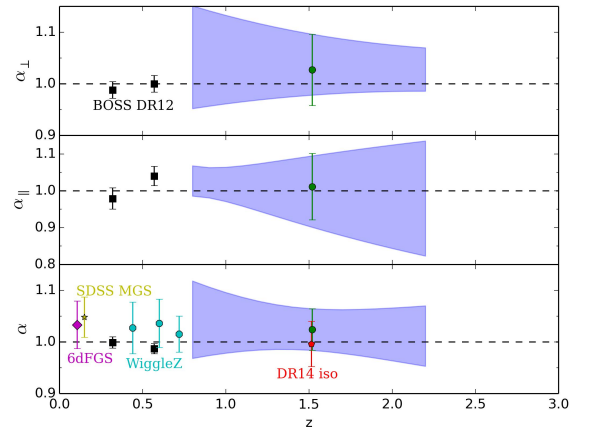


Figure 6. A 68% CL reconstruction of the time evolution of α_\perp , α_{\parallel} and the isotropic α derived from α_\perp , α_{\parallel} (blue bands), and the measurement at the effective redshift without z-weights (green circles with error bars), in comparison with other measurements in the literature including: BOSS DR12 (Alam et al. 2017), eBOSS DR14 isotropic BAO constraint (Ata et al. 2018), WigglyZ (Kazin et al. 2014) and MGS (Ross et al. 2015)

constraint on α_{\parallel} can be diluted when both α_0 and α_1 become better constrained (α_{\parallel} is essentially a product of α_0 and α_1);

- The parameter α_1 is consistent with zero within the error bars, that there is no evidence for the time evolution of α from the DR14 quasar sample. Fig 6, shows a 68% CL reconstruction of the evolution history of α_\perp , α_{\parallel} and α in the redshift range of $0.8 < z < 2.2$. For a comparison, we display the constraint without the redshift weights, along with other published constraints in the literature, including the BOSS result from (Alam et al. 2017), eBOSS DR14 isotropic BAO constraint (Ata et al. 2018), the WigglyZ (Kazin et al. 2014) and the MGS (Ross et al. 2015) result;

- Extending the k range to $0.3 h \text{ Mpc}^{-1}$ slightly improves the constraints, i.e. the extension tightens the constraints on α_\perp , α_{\parallel} and α by 7%, 2% and 5%, respectively, and the degeneracy among BAO parameters is slightly reduced. The constraint on α , 1.021 ± 0.038 , is fully consistent with the BAO analysis using the same data sample (Ata et al. 2018);

- The reduced χ^2 in all cases is reasonably consistent with unity, meaning that we are neither overfitting or underfitting the data.

Redshift	$D_M(r_{d,\text{fid}}/r_d)$ [Mpc]	$H(r_{d,\text{fid}}/r_d)$ [kms ⁻¹ Mpc ⁻¹]	$D_V(r_{d,\text{fid}}/r_d)$ [Mpc]
$z_1 = 0.8$	3020 ± 258	104 ± 4.4	2759 ± 198
$z_2 = 1.0$	3560 ± 292	118 ± 5.6	3179 ± 180
$z_3 = 1.5$	4459 ± 275	159 ± 15	3940 ± 155
$z_4 = 2.0$	5479 ± 239	207 ± 29	4432 ± 223
$z_5 = 2.2$	5755 ± 235	227 ± 35	4580 ± 265

Table 3. The derived BAO distance indicators from Table 2.

From our result, we derive the commonly used BAO distance indicators $D_M(r_{d,\text{fid}}/r_d)$, $H(r_{d,\text{fid}}/r_d)$ and $D_V(r_{d,\text{fid}}/r_d)$ at five effective redshifts (Table 3), and the correlations of $D_M(r_{d,\text{fid}}/r_d)$ and $H(r_{d,\text{fid}}/r_d)$ are shown in APPENDIX A. As these are derived from constraints on only two parameters of α_0 and α_1 , the error bars of these quantities are highly correlated, *i.e.*, the covariance matrix is close to singular. Therefore these constraints are only suitable for comparison with other measurements at similar redshifts. For cosmological parameter estimation, we recommend the readers to use the result reported in Table 2 instead.

5 CONCLUSION AND DISCUSSIONS

We have developed a method to extract the tomographic BAO information from wide-angle redshift surveys. Working in Fourier space, we analytically derive optimal redshift weights for power spectra multipoles for the eBOSS DR14 quasar sample, which covers the redshift range of $0.8 < z < 2.2$. We build a framework in which the redshift-weighted power spectra multipoles can be combined to yield improvement on the BAO constraint, and apply our pipeline to the DR14 quasar sample after validating it using the EZ galaxy mock catalogues.

Our work yields an anisotropic BAO measurement at the effective redshift of 1.52: $\alpha_{\perp} = 1.037 \pm 0.059$ and $\alpha_{\parallel} = 0.998 \pm 0.097$, and an isotropic BAO measurement of $\alpha = 1.024 \pm 0.040$. Compared to the case without the redshift weights, the constraint on the isotropic BAO dilation parameter gets tightened by 17%.

Another BAO analysis with redshift weights is performed in a companion paper (Zhu et al. 2018), which differs from ours primarily regarding the fact that Zhu et al. (2018) performs the analysis in configuration space. In this sense, our results are complementary to each other. The results from this work are generally consistent with that in Zhu et al. (2018).

Two additional companion papers (Zhao et al. 2018; Ruggeri et al. 2018) perform joint BAO and RSD analysis with the optimal redshift weights in Fourier space. Our BAO constraints are generally consistent with each other within the error budget.

The method developed in this work can be directly applied to the complete eBOSS sample when the survey finishes, and to future deep redshift surveys including DESI (DESI Collaboration et al. 2016) and Euclid (Laureijs et al. 2011).

ACKNOWLEDGEMENTS

DW, GB and YW are supported by NSFC Grants 1171001024 and 11673025. GBZ is also supported by a Royal Society Newton Advanced Fellowship, hosted by University of Portsmouth. YW is

supported by a NSFC Grant No. 11403034, and by a Young Researcher Grant of National Astronomical Observatories, Chinese Academy of Sciences.

Funding for SDSS-III and SDSS-IV has been provided by the Alfred P. Sloan Foundation and Participating Institutions. Additional funding for SDSS-III comes from the National Science Foundation and the U.S. Department of Energy Office of Science. Further information about both projects is available at www.sdss.org. SDSS is managed by the Astrophysical Research Consortium for the Participating Institutions in both collaborations. In SDSS-III these include the University of Arizona, the Brazilian Participation Group, Brookhaven National Laboratory, Carnegie Mellon University, University of Florida, the French Participation Group, the German Participation Group, Harvard University, the Instituto de Astrofísica de Canarias, the Michigan State / Notre Dame / JINA Participation Group, Johns Hopkins University, Lawrence Berkeley National Laboratory, Max Planck Institute for Astrophysics, Max Planck Institute for Extraterrestrial Physics, New Mexico State University, New York University, Ohio State University, Pennsylvania State University, University of Portsmouth, Princeton University, the Spanish Participation Group, University of Tokyo, University of Utah, Vanderbilt University, University of Virginia, University of Washington, and Yale University.

The Participating Institutions in SDSS-IV are Carnegie Mellon University, Colorado University, Boulder, Harvard-Smithsonian Center for Astrophysics Participation Group, Johns Hopkins University, Kavli Institute for the Physics and Mathematics of the Universe Max-Planck-Institut fuer Astrophysik (MPA Garching), Max-Planck-Institut fuer Extraterrestrische Physik (MPE), Max-Planck-Institut fuer Astronomie (MPIA Heidelberg), National Astronomical Observatories of China, New Mexico State University, New York University, The Ohio State University, Penn State University, Shanghai Astronomical Observatory, United Kingdom Participation Group, University of Portsmouth, University of Utah, University of Wisconsin, and Yale University.

This work made use of the facilities and staff of the UK Sciama High Performance Computing cluster supported by the ICG, SEP-Net and the University of Portsmouth. This research used resources of the National Energy Research Scientific Computing Center, a DOE Office of Science User Facility supported by the Office of Science of the U.S. Department of Energy under Contract No. DE-AC02-05CH11231.

APPENDIX A: THE CORRELATION MATRIX

$$\begin{array}{cccccc}
 D_M(z_1) & H(z_1) & D_M(z_2) & H(z_2) & D_M(z_3) & H(z_3) \\
 1.000 & 0.565 & 0.997 & -0.106 & 0.948 & -0.657 \\
 & 1.000 & 0.623 & 0.761 & 0.798 & 0.252 \\
 & & 1.000 & -0.034 & 0.969 & -0.600 \\
 & & & 1.000 & 0.216 & 0.820 \\
 & & & & 1.000 & -0.382 \\
 & & & & & 1.000 \\
 \\
 D_M(z_4) & H(z_4) & D_M(z_5) & H(z_5) & & \\
 0.767 & -0.760 & 0.643 & -0.779 & D_M(z_1) & \\
 0.963 & 0.108 & 0.995 & 0.781 & H(z_1) & \\
 0.812 & -0.710 & 0.697 & -0.731 & D_M(z_2) & \\
 0.556 & 0.728 & 0.693 & 0.707 & H(z_2) & \\
 0.931 & -0.513 & 0.853 & -0.539 & D_M(z_3) & \\
 -0.020 & 0.989 & 0.155 & 0.985 & H(z_3) & \\
 1.000 & -0.165 & 0.985 & -0.195 & D_M(z_4) & \\
 & 1.000 & 0.010 & 1.000 & H(z_4) & \\
 & & 1.000 & -0.020 & D_M(z_5) & \\
 & & & 1.000 & H(z_5) &
 \end{array} \quad (A1)$$

The correlation matrix of Fig 3.

REFERENCES

- Abolfathi B. et al., 2017, ArXiv e-prints: 1707.09322
Alam S. et al., 2017, MNRAS, 470, 2617
Alam S., et al., 2017, Mon. Not. Roy. Astron. Soc., 470, 2617
Alcock C., Paczynski B., 1979, Nature, 281, 358
Ata M., et al., 2018, Mon. Not. Roy. Astron. Soc., 473, 4773
Bianchi D., Gil-Marín H., Ruggeri R., Percival W. J., 2015, MNRAS, 453, L11
Blanton M. R. et al., 2017, AJ, 154, 28
Chuang C.-H., Kitaura F.-S., Prada F., Zhao C., Yepes G., 2015, Mon. Not. Roy. Astron. Soc., 446, 2621
Cole S. et al., 2005, MNRAS, 362, 505
Croom S. M. et al., 2005, MNRAS, 356, 415
Dawson K. S. et al., 2016, AJ, 151, 44
Dawson K. S. et al., 2012, ArXiv e-prints:1208.0022
Dawson K. S., et al., 2016, Astron. J., 151, 44
DESI Collaboration et al., 2016, ArXiv e-prints
Eisenstein D. J. et al., 2011, AJ, 142, 72
Eisenstein D. J. et al., 2005, ApJ, 633, 560
Feldman H. A., Kaiser N., Peacock J. A., 1994, ApJ, 426, 23
Gunn J. E., et al., 2006, Astron. J., 131, 2332
Hartlap J., Simon P., Schneider P., 2006, Astron. Astrophys., [Astron. Astrophys.464,399(2007)]
Kazin E. A. et al., 2014, Monthly Notices of the Royal Astronomical Society, 441, 3524
Laureijs R. et al., 2011, ArXiv e-prints
Laurent P. et al., 2017, J. Cosmology Astropart. Phys., 7, 017
Lewis A., Bridle S., 2002, Phys. Rev. D, 66, 103511
Linder E. V., 2005, Phys. Rev. D, 72, 043529
Myers A. D. et al., 2015, ApJS, 221, 27
Pâris I. et al., 2017, A&A, 597, A79
Percival W. J., et al., 2014, Mon. Not. Roy. Astron. Soc., 439, 2531
Perlmutter S. et al., 1999, ApJ, 517, 565
Riess A. G. et al., 1998, AJ, 116, 1009

- Ross A. J., Samushia L., Howlett C., Percival W. J., Burden A., Manera M., 2015, Monthly Notices of the Royal Astronomical Society, 449, 835
Ruggeri R., Percival W. J., Gil-Marín H., Zhu F., Zhao G.-B., Wang Y., 2017, MNRAS, 464, 2698
Ruggeri R., et al., 2018, Arxiv
Sefusatti E., Crocce M., Scoccimarro R., Couchman H. M. P., 2016, MNRAS, 460, 3624
Smee S. A. et al., 2013, AJ, 146, 32
Wang Y. et al., 2017, MNRAS, 469, 3762
Zhao G.-B., Crittenden R. G., Pogosian L., Zhang X., 2012, Physical Review Letters, 109, 171301
Zhao G.-B. et al., 2017a, Nature Astronomy, 1, 627
Zhao G.-B. et al., 2017b, MNRAS, 466, 762
Zhao G.-B., et al., 2017, Mon. Not. Roy. Astron. Soc., 466, 762
Zhao G.-B., et al., 2018, Arxiv
Zhu F., Padmanabhan N., White M., 2015, Mon. Not. Roy. Astron. Soc., 451, 236
Zhu F., Padmanabhan N., White M., Ross A. J., Zhao G., 2016, Monthly Notices of the Royal Astronomical Society, 461, 2867
Zhu F., Padmanabhan N., White M., Ross A. J., Zhao G.-B., 2016, MNRAS, 461, 2867
Zhu F., et al., 2018, Arxiv